Research Article | Vol. 28, No. 26 / 21 December 2020 / Optics Express 39606

Optics EXPRESS

Impact of laser frequency noise on high-extinction optical modulation

GAVIN N. WEST,[1,*] WILLIAM LOH,[2] DAVE KHARAS,[2] AND RAJEEV J. RAM[1]

[1] Massachusetts Institute of Technology, 77 Massachusetts Ave., Cambridge, MA 02139, USA
[2] MIT Lincoln Laboratory, 244 Wood Street, Lexington, MA 02421, USA
[*] westgn@mit.edu

Abstract: In present literature on integrated modulation and filtering, limitations in the extinction ratio are dominantly attributed to a combination of imbalance in interfering wave amplitude, instability of control signals, stray light (e.g., in the cladding), or amplified spontaneous emission from optical amplifiers. Here we show that the existence of optical frequency noise in single longitudinal mode lasers presents an additional limit to the extinction ratio of optical modulators. A simple frequency-domain model is used to describe a linear optical system's response in the presence of frequency noise, and an intuitive picture is given for systems with arbitrary sampling time. Understanding the influence of frequency noise will help guide the design choices of device and system engineers and offer a path toward even higher-extinction optical modulators.

1. Introduction

The past decade has seen the emergence of integrated photonics in exotic applications. Proposals and demonstrations in quantum key distribution (QKD) transceivers [1], chip-scale optical atomic clocks [2], and scalable quantum computing and quantum networks [3–7] have broadened the field beyond traditional silicon-based datacomm devices. These specialized applications carry new device constraints: footprint is often less constrained, operating wavelengths may span the ultraviolet to mid-infrared, and active components may trade ultra-fast speed for precise control [8–10]. In particular, quantum optics-adjacent systems have stringent requirements on spectro-temporal control of light, down to the individual photon level. Contrasting with telecom-focused silicon photonics, applications relying on the quantum mechanical behavior of light are *fragile* — every photon matters.

For example, the future of generalized quantum information processing (QIP) relies on reducing error rates to the point where error correcting codes can be implemented [11,12]. In the field of trapped ion QIP, these errors can be introduced by inadequate suppression of the laser signals used to manipulate the qubit ions. Analogous requirements exist in photon-based QIP, where leading on-chip sources of nonclassical light use a strong pump to generate signal photons; the pump must be strongly filtered to prevent swamping out the signal. Estimates for the required pump suppression range from 90 to 130 dB [13–16]. Additionally, techniques such as "decoy state" quantum key distribution are predicated on the ability to create so-called vacuum states with zero photons transmitted in a time bin [17]. Spurious photons transmitted during this time bin degrades the link security. An important metric for modulators in these applications is then the extinction ratio (ER), the ratio of power transmitted in the "on" and "off" state. Many approaches have been developed to address this high ER demand, from cascaded lattice filters to coupled rings to tunable cascaded Mach-Zehnder interferometers [14–16,18–20]. From previous results in literature, it is clear there are two branches of success: (ultra) high-ER static filters, and (very) high-ER active modulators. Further, the best example of high-ER filters involves two separate chips each with a large consumed area and substantial insertion loss.

#413850 https://doi.org/10.1364/OE.413850
Journal © 2020 Received 4 Nov 2020; revised 2 Dec 2020; accepted 7 Dec 2020; published 15 Dec 2020

Optics EXPRESS

To make progress in reducing device size, or increasing ER, it is necessary to understand what limits ER and how a specific device architecture is affected. The vast majority of integrated photonic modulators are based on destructive interference between two optical waves and as such are exquisitely sensitive to imbalance in the wave amplitudes. As a result, the largest and most well-understood factor in ER is a result of stochastic fabrication variations — variance in geometric parameters, sidewall roughness [21], and perturbations in material properties such as refractive index. Such imperfections manifest as variation in splitting ratios and propagation loss which imbalance the interfering wave amplitudes. Other factors include stray photons which propagate in the cladding layers, instability of the modulation control signal, polarization impurity, and spurious signal from amplified spontaneous emission (ASE) [13,14,19,22].

In this work we discuss the behavior of optical modulators in the presence of laser frequency noise and show that such noise places a fundamental limit on the ER of a filter or modulator. All real, single-frequency lasers exhibit a characteristic spectral distribution of power in the optical frequency domain, a consequence of inescapable physical processes. This spectral distribution ("lineshape") has been studied in the context of channel crosstalk frequency-multiplexed communication networks [23,24]. Similarly, the behavior of resonators in the presence of laser frequency and cavity resonance fluctuations — the dual process of laser frequency fluctuation — has been analyzed in detail [25]. However, these works do not address the impact on extinction ratio. Here we expand the discussion of optical device behavior with finite-linewidth sources and show that this distribution of power can limit the time-averaged ER markedly. We discuss how different modulator architectures are affected, and use a simple frequency-domain model to accurately predict system response. Analytic solutions are given for the extinction of Mach-Zehnder and ring resonator modulators probed with a Lorentzian laser. We experimentally validate the model and demonstrate the importance of the exact laser lineshape on the extinction ratio.

2. Modeling

Consider an oscillating, single-frequency, linearly-polarized electric field without amplitude noise. We can express its time evolution through its phase $\Phi(t)$ as

$$\vec{E}(\vec{r},t) = \vec{E}(\vec{r})\exp\left[j\Phi(t)\right] \tag{1}$$

$$= \vec{E}(\vec{r})\exp\left[j\omega_0 t + j\phi(t)\right]. \tag{2}$$

where $\phi(t)$ are zero-mean phase fluctuations of the field observed from a reference frame rotating at the carrier frequency $\omega_0 = 2\pi\nu_0$. The value of $\phi(t)$ varies in time as a result of both stochastic processes, such as spontaneous emission, and environmental perturbations, such as temperature fluctuations or mechanical vibrations. These phase fluctuations can also be expressed as frequency fluctuations $\delta\nu(t)$, up to a global phase, through a time derivative $\delta\nu(t) = 1/2\pi\partial\phi(t)/\partial t$. For the purposes of this work, *phase noise* and *frequency noise* are taken to be synonymous, and frequency noise is used preferentially due to its easily-grasped intuition and mathematical representation. Based on situation, lasers are often quoted in terms of "linewidth" and "center frequency stability". These are not distinct as they are based on the time scale of measurement — this will be further elucidated, below. We make the choice to define a time-invariant center frequency with all fluctuations around this value.

Next consider using this signal to interrogate a device whose transfer function has a local minimum. Figure 1(a) illustrates the signal fluctuating around minimum of the transmission function. Clearly, in the presence of frequency noise, there is some non-zero integrated time during which the signal's instantaneous frequency $\nu_0 + \delta\nu(t)$ is away from the local minimum. As a result there is a greater time-averaged power transmission than would be observed if a truly single-frequency signal were used. This is the basis of our claim: The presence of laser frequency

Optics EXPRESS

noise results in higher-than-predicted transmitted power around a transmission null, which places a limit on the measured extinction ratio.

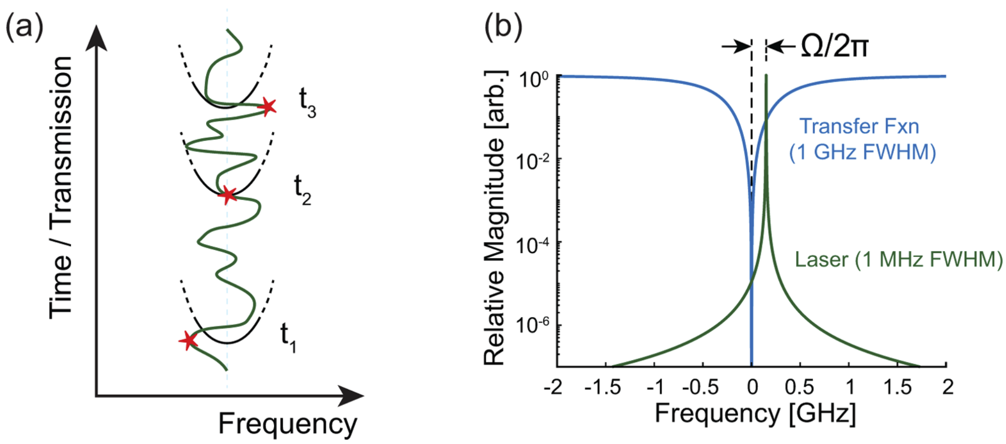

Fig. 1. (a) A cartoon illustrating how frequency fluctuations sample multiple points on a transfer function, over time. The magnitude of the fluctuation is exaggerated greatly for clarity. (b) The long-time-average picture, where frequency noise is represented by the resulting power distribution function — a lineshape. Even for very disparate filter and signal FWHM, the decaying Lorentzian-like tails are poorly suppressed. When the near-carrier power is highly suppressed, the power carried in these tails becomes a significant of the transmission. The filter here has a true zero at its center wavelength, and the lineshape is normalized to unity power. Ω is the offset between signal and filter center frequencies.

To describe this limitation rigorously we must quantify the amount of time the signal spends at each point on the transfer function. Thankfully a mathematical construction describing this already exists: the signal lineshape. Lineshape describes the spectral distribution of power (over some time scale) and is analogous to a probability distribution function of the instantaneous frequency position in time. The short, high-frequency excursions of the signal become slowly-decaying spectral tails, shown in Fig. 1(b). While power contained in these tails is typically ignored it becomes an appreciable contribution to total transmission when the near-carrier power is highly suppressed. If the signal's lineshape $L(\omega)$ and the device's transmission function $H(\omega)$ are known, the total transmitted power is the integral of their product. With an offset Ω between some reference frequency on each (e.g. the center frequencies) it becomes the cross-correlation between signal and transmission function

$$T_{eff}(\Omega) = \int_{-\infty}^{\infty} H(\omega)L(\omega - \Omega)d\omega. \tag{3}$$

While many simple descriptions exist for $L(\omega)$, such as Lorentzian and Voigt functions which are typically specified by their full-width at half-maximum (FWHM), these have subtle approximations built-in. In general, real noise processes are complex and do not yield analytic lineshapes. However, if the signal's frequency noise spectra is measured (there are many techniques, see [26–29]) the corresponding lineshape can be calculated numerically. We will refer to the FWHM of this line shape this as the "FT linewidth". Plentiful literature discusses the details of the noise-to-lineshape calculation [29–32]. In Appendix A we condense these calculations so far as is relevant for this work. The important takeaway is that there is no standard definition of "linewidth" — confusing quoted values in literature and from commercial vendors — and the single-valued metric is not always sufficient to describe the signal's behavior. One of the most common definitions is referred to as the "fundamental" or "Lorentzian" linewidth, which stems from the well-known result of Schawlow and Townes [33]. This definition assumes a white noise spectrum whose magnitude is extracted from the asymptotic limit at high frequencies [34–36], where technical noise sources are assumed to be negligible. By ignoring technical noise — which is typically many orders of magnitude larger than the floor set by spontaneous emission — the fundamental linewidth can give much smaller values than other metrics. Another common definition is the "integral" linewidth [37], which computes the frequency above which the integrated phase noise is 1 radian. While the integral linewidth does take the real phase noise spectrum into account, like any definition of "linewidth" it is blind to noise content at lower frequencies. These definitions are then most useful in applications where the measurement period is shorter than the inverse linewidth. All three definitions here ("fundamental/Lorentzian", "integral", and "FT") converge to the same value for white noise. In Sec. 3 we demonstrate that low-frequency distortions of the lineshape can be important for accurately predicting system response.

For the sake of obtaining analytic results with Eq. (3), we will start by treating the lineshape as Lorentzian with a given full-width at half-maximum. This corresponds to a frequency noise spectrum which is entirely white, as would be approximately true for a laser whose noise is limited by spontaneous emission. Transfer functions for common modulators, based on Mach-Zehnder Interferometer (MZI) and "all-pass" ring resonators (MRR), are given by [38,39]

$$H_{MZI}(\omega) = \frac{1}{2}\left[1 - \cos\left(\pi\frac{(\omega-\omega_0)}{\Delta\omega_{FWHM}}\right)\right] \tag{4}$$

$$H_{MRR}(\omega) = \frac{(\omega-\omega_0)^2}{(\Delta\omega/2)^2 + (\omega-\omega_0)^2}. \tag{5}$$

It is worth pointing out that for MZI structures with balanced path lengths, the transfer function's curvature results from the achromaticity of the beamsplitter elements and is not necessarily sinusoidal. For broadband devices, where the effects relevant to this work are confined to within 1 FWHM, a fitted sinusoid is a suitable approximation for the real transfer function.

Equations (4) and (5) assume perfect "intrinsic" extinction — the smallest function value computed with an infinitely narrow source is zero — and can be easily modified to account for a non-zero minimum value. For a Lorentzian lineshape with unit power, analytic solutions exist for the cross-correlation with both MRR and MZI transfer functions:

$$T_{eff,MRR}(\Omega) = \frac{\Delta\omega_L^2 + \Delta\omega_F\Delta\omega_L + 4\Omega^2}{(\Delta\omega_F + \Delta\omega_L)^2 + 4\Omega^2} \tag{6}$$

$$T_{eff,MZI}(\Omega) = \frac{1}{2}\left[1 + \cos\left(\frac{\pi\Omega}{\Delta\omega_F}\right)\left(\sinh\left(\frac{\pi\Delta\omega_L}{2\Delta\omega_F}\right) - \cosh\left(\frac{\pi\Delta\omega_L}{2\Delta\omega_F}\right)\right)\right] \tag{7}$$

where $\Delta\omega_L$ is the signal FWHM and $\Delta\omega_F$ is the transfer function FWHM. It is clear that even for $\Omega = 0$ there is nonzero minimum transmission in both cases, and that the value is a function of the ratio of signal and transfer function FWHM. Figures 2(a) and (b) illustrate these results for several signal FWHM. For the realistic case of finite "intrinsic" extinction, the transmission curve becomes a function of the lineshape — naturally, a very (relatively) narrow signal will more faithfully represent the filter while a broad signal will behave similarly to the analytic results above.

A naïve solution would be to lock the signal to the local minimum [40], suppressing the high-frequency-offset excursions. The most common techniques to lock to a local minimum involve frequency dithering either the signal or the modulator itself. In both cases sidebands are generated which are spectrally offset from the transmission null, resulting in unwanted power transmission. Other approaches such as side-of-fringe do not lock to the local minimum, again

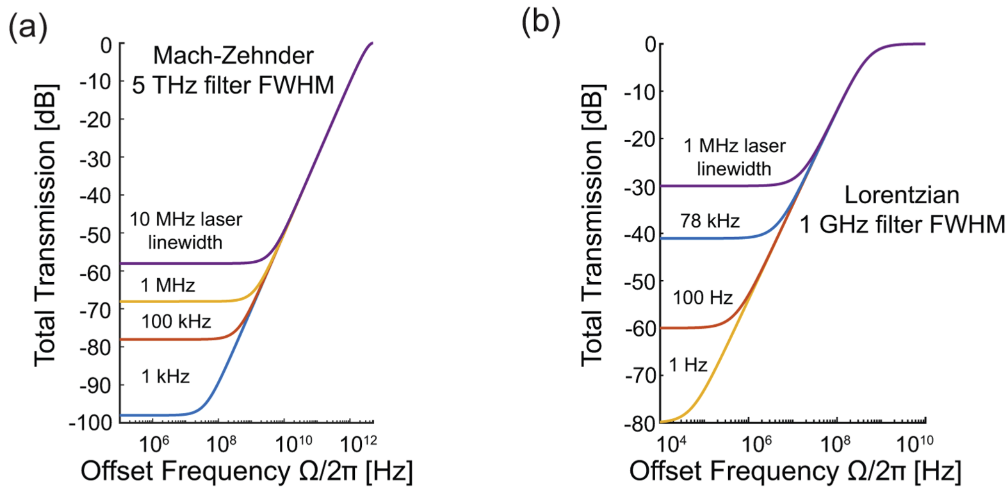

Fig. 2. Analytic solutions for the cross-correlation of a Lorentzian lineshape of various FWHM with (a) a Mach-Zehnder-like (sinusoidal) transfer function with 5 THz FWHM and (b) a ring resonator-like (Lorentzian) transfer function with 1 GHz FWHM.

resulting in poor extinction. Furthermore, any locking or work done to reduce low frequency drift is equivalent to adding a phase term $\phi'(t)$ to the exponent of Eq. (2) which reduces the variance of fluctuations, that is $\langle(\phi'(t) + \phi(t))^2\rangle < \langle\phi(t)^2\rangle$. This is equivalent to simply using a laser which has lower phase noise and the theory we develop here suitably describes the locked system.

3. Experimental validation

We created a variable-linewidth laser using the setup shown in Fig. 3(a). A commercial C-band tunable semiconductor laser (Santec TSL-550) is fed through a broadband electro-optic phase modulator (EOM, EOSpace 20 GHz BW), which is in turn driven by a broadband white noise generator (Toptica Laser Coherence Controller (LCC)). An in-line attenuator controls the electrical power injected into the EOM and an in-line low pass filter (30 MHz cutoff frequency) is used to control the shape of the electrical signal. This setup permits independent control of the center frequency and (additive) noise spectrum. For simulating more complex noise spectra, a shaped RF input (e.g. from an arbitrary waveform generator or a passively-filtered noise source) can be used in place of the simple white noise generator. As long as the desired noise spectra can be achieved by adding noise, this allows arbitrary manipulation of the laser noise/lineshape. Here, laser frequency noise spectra for various injected RF noise powers are measured using an unbalanced MZI approach [26] with an HP89410A vector signal analyzer and given in Fig. 3(b). We used this laser to measure a filter's transmission, at each injected noise level. To verify that TE-TM polarization coupling was not occurring in the phase modulator, we measured a set of resonances at various RF input and found the optimum polarization to maximize the resonance extinction; the optimal paddle positions were found to be independent of RF power.

Our filter was a ring resonator with a ~ 7 MHz full-width at half-maximum and 3 GHz free spectral range. By sweeping the laser wavelength and observing the transition from an under-coupled to over-coupled state, we found the ring was near critically-coupled around 1580 nm. The highest-extinction resonance was located manually, and all subsequent measurements performed on this resonance. We observed a maximum 19 dB ER, and this value was insensitive when neighboring resonances were measured. This is consistent with our laser's minimum achievable noise — no noise injected via the EOM — and the theory described in Section 2,

Optics EXPRESS

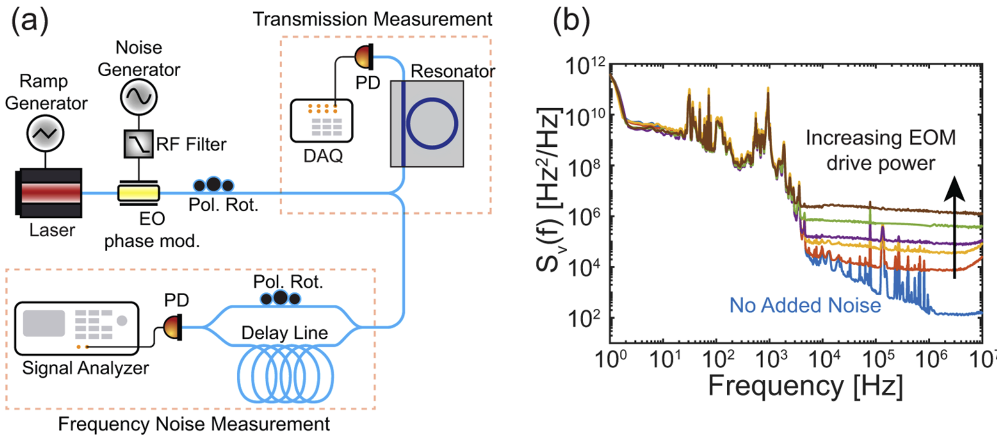

Fig. 3. (a) Our experimental setup, showing the variable-noise laser alongside the measured resonator and noise-measurement apparatus. PD = Photodiode, DAQ = Data Acquisition Module, Pol. Rot. = Polarization Rotation paddles. (b) Measured single-sided frequency noise spectra at several RF (noise) power levels.

though in this section we focus on the trends.We used an external ramp generator (Vescent D2-125 laser servo) to sweep the laser's center frequency over the resonance at a 50 Hz repetition rate and recorded the photodiode (PD, Thorlabs PDA10CD) signal on a 1.25 MSamp/sec 16 bit data acquisition board (DAQ, National Instruments USB-6251), examples of which are shown in Fig. 4(a). The extinction ratio was extracted from these transmission curves. Without attenuation, approximately 50 mW of RF noise power is injected into the EOM. Because the laser frequency was dynamically swept during the measurement it is necessary to check that the reduced extinction is not a result of an averaging effect from the injected frequency ramp. Based on our sweep rate, frequency span, and sampling rate, we estimate that without the effects of finite laser linewidth the extinction floor would be $\sim$ 45 dB (near the noise floor of the ADC resolution).

The noise spectra in Fig. 3(b) are used to compute corresponding lineshapes using the process described in Appendix A., shown in Fig. 4(c), with the label corresponding to the curve FWHM. We choose to report the FWHM to illustrate the difference between the fundamental linewidth (425 Hz), the integral linewidth (79 kHz), and the FWHM linewidth (260 kHz). Additionally, non-Lorentzian pedestals form at higher injected noise power and begin to fall off at 30 MHz where the injected noise is reduced by a low-pass filter. It is worth noting that because the laser's center frequency is artificially swept over the resonance at some rate, the low frequency noise processes manifest as center frequency shifts of the measured transmission function. We aligned the resonances in data processing and found this was equivalent to ignoring frequency noise below $\sim$ 3 kHz. Thus, the transformed lineshapes in Fig. 4(c) represent the noise in Fig. 3(b) above 3 kHz. Numerically convolving these lineshapes as expressed in Eq. (3) gives a prediction of the maximum extinction, which is compard to the measured values in Fig. 4(b). The predicted values match the trend in measured values extremely well. For comparison we analytically compute the expected trend if the laser lineshape were Lorenzian, with an equivalent FWHM value. This result demonstrates the dependence of behavior on lineshape — the non-Lorentzian features changes both the value of extinction for a given linewidth, and the curvature of the trend. While these pedestals are a consequence of the injected noise and low-pass filtering, similar frequency noise structures (and thus features on the lineshape) can be caused by, for example, mechanical resonances in an external cavity, feedback servo bumps, phase-amplitude coupling, carrier injection/optical pump noise, and relaxation oscillation resonances.

Optics EXPRESS

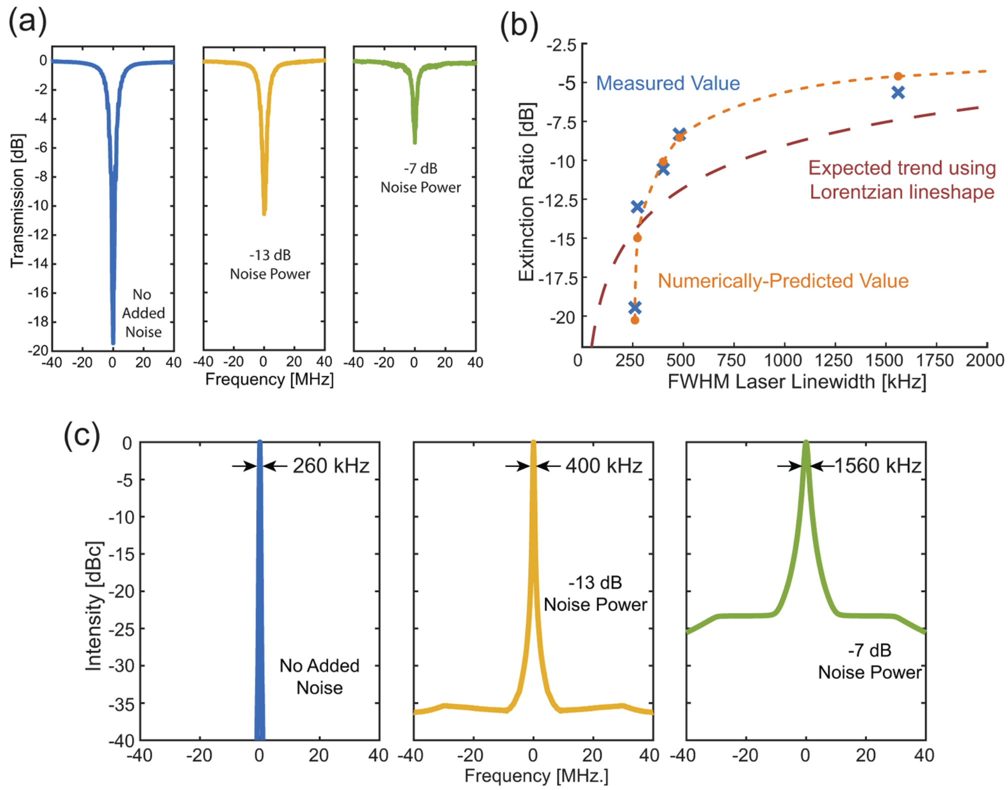

Fig. 4. (a) Example measured transmission spectra, at various levels of injected noise. (b) The measured extinction ratio (blue crosses) and the numerically-predicted values using the computed lineshapes from (a) (orange dots), with a curve fit to illustrate the trend (orange dashed line). Using a cross-correlation with analytic filter/signal functions for a given laser FWHM (red dashed line), does not follow the experimental data, and diverges quite strongly at small FWHM linewidths. (c) Calculated laser lineshapes using the Fourier transform of the frequency noise spectrum. The given widths are the FWHM of these spectra.

4. Discussion

While the main result here is the extinction cap induced by laser frequency noise and its dependence on lineshape, there are several interesting implications.

The first is that, over repeated measurements, the average extinction ratio is set by the noise properties of the laser and filter shape and is independent of sampling time. While fast sampling times only observe higher frequency noise (typically smaller in magnitude than low-frequency noise), resulting in a narrower "sampled" linewidth, the low frequency noise components then correspond to carrier frequency drift. Figure 5(a) provides an intuitive picture for this behavior. As a result, the average transmission of samples taken over a time period T will converge to the result obtained using a lineshape calculated from frequency noise measured down to frequencies $\propto 1/T$ and the theory described above.

The second takeaway is not immediately intuitive: cascading multiple identical filters *does not increase extinction additively* (in dB). This can be seen easily by imagining a band-stop filter with perfect suppression over some finite bandwidth, and perfect transmission outside that bandwidth. Serially linking these filters does not change the overall transfer function (if the filters are aligned) and thus does not change the transmitted power. As a more practical example, cascading two

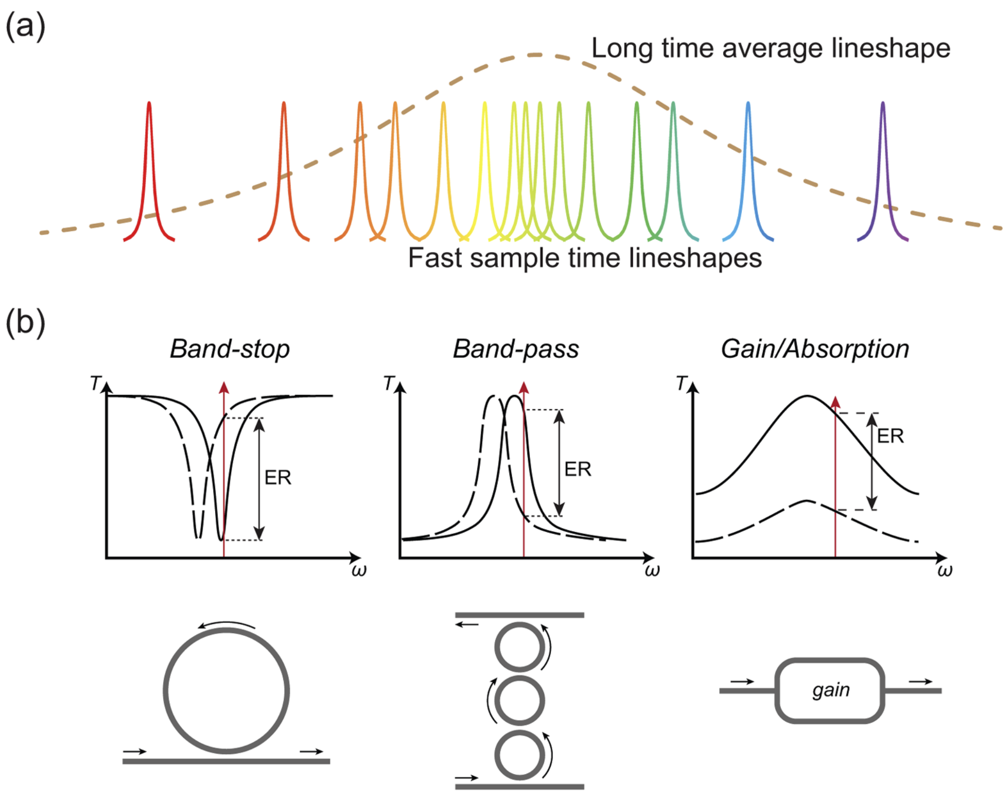

Fig. 5. (a) An illustration comparing the lineshape calculated with low frequency noise, and the spread of effective lineshapes with a short sampling time. The distribution of fast-sampled curves cumulatively average to the "long time average" curve. (b) The common filter shapes used to create optical modulators. The device cartoons represent integrated photonic devices which produce such filter shapes: from left to right an "all-pass" ring resonator, a multi-pole coupled resonator observing the drop port, and an element such as an optical amplifier or electro-absorption material.

Lorentzian filters with infinite intrinsic extinction (but finite real extinction, limited by the laser's noise) improves extinction by only about 3 dB. Additional filters contribute incrementally less and less suppression, asymptotically approaching 5.1 dB for each tenfold increase in number of filters. Of course, linear system theory is still applied when the spectral decomposition of the signal is known, as is done here, but this can be difficult in practice. Experimentally, transmission curves are measured against center frequency without taking the signal's bandwidth into account. Thus, the observed transmission curve does not exactly represent the measured device, though this effect is of course dependent on the relationship between the filter's linewidth, its intrinsic extinction, and the signal linewidth. In cases where the intrinsic extinction is limiting ($\Delta\omega_L << \Delta\omega_F$) the single-frequency source approximation is good and the extinctions will approximately add. When the signal bandwidth is limiting, the effect may be minimal.

This framework also applies itself to another fundamental noise source: thermorefractive noise. Thermal fluctuations in the local refractive index cause the center frequency of any interferometric filter to move in time. In the reference frame of the filter these fluctuations appear on the incident signal and thus the analysis introduced above can be applied. References [41] and [42] provide excellent introductions to thermorefractive noise, particularly as it relates to induced frequency micro and nano-scale optical resonators.

Optics EXPRESS

In practice, this understanding also helps to inform modulator design when high ERs are desired. Our discussion has focused on band-stop filter shapes, as the prevalence of ring and MZI modulators make them pertinent. There are three general classes of transfer functions used for modulators, illustrated in Fig. 5(b) with cartoons of integrated optical devices which result in such transfer functions. Clearly, the band-stop filters are more susceptible than band-pass filters to transmitting power away from the carrier; the band-pass filter response naturally suppress the tails outside the pass band, limiting the effect to the integrated power over this (relatively narrow) width. Similarly, gain/absorption-based structures are typically wideband — flat response over hundreds of GHz or a few nanometers, in this context — and are relatively less affected.

5. Conclusion

Here we have introduced laser frequency noise as a contributor to extinction ratio limits in optical modulators and filters. Even for single-frequency lasers, stochastic fluctuations in the instantaneous frequency give rise to a finite linewidth which is unevenly suppressed by common modulator architectures. A simple mathematical model is introduced which predicts the average extinction ratio of a modulator over many samples and which is valid for arbitrary lineshapes/frequency noise spectra. We validate the theory with an experiment, using a variable-linewidth laser and a common ring resonator. We believe this new understanding will aid the development of ultra-high-extinction modulators.

Appendix A. Frequency noise and lineshape

Before discussing its effect on modulator performance, a description of frequency noise and its relationship to laser lineshape is needed. A variety of literature is available which discusses common noise processes [29,32,33,43], metrics for characterizing noise (e.g., definitions of linewidth) [30,37,44], and techniques for measuring this noise [26–29]. Portions of this are briefly reiterated, here.

Returning to Eq. (2), consider an oscillating, single-frequency, linearly-polarized electric field without amplitude noise. We can express its time evolution through its phase $\Phi(t)$ as

$$\begin{aligned}\vec{E}(\vec{r},t) &= \vec{E}(\vec{r})\exp\left[j\Phi(t)\right]\\ &= \vec{E}(\vec{r})\exp\left[j\omega_0 t + j\phi(t)\right]\end{aligned}$$

where $\phi(t)$ are zero-mean, Gaussian-distributed phase fluctuations of the field observed from a reference frame rotating at the carrier frequency $\omega_0 = 2\pi\nu_0$. These phase fluctuations can also be expressed as frequency fluctuations $\delta\nu(t)$, up to a global phase, through a time derivative $2\pi\delta\nu(t) = \partial\phi(t)/\partial t$. The relationship between frequency fluctuations and the lineshape are described by the Wiener-Khinchin theorem, which states that the spectral power distribution $S_E(f)$ of a process is given by the Fourier transform of the processes' autocorrelation $R_{EE}(\tau)$:

$$S_E(f) = \mathcal{F}\left\{R_{EE}(\tau)\right\}. \tag{8}$$

The autocorrelation is related to the fluctuation in phase by

$$R_{EE}(\tau) = \langle E(t)E^*(t-\tau)\rangle \tag{9}$$

$$\propto E_0^2 e^{j2\pi\nu\tau} e^{-\langle\Delta\phi(\tau)^2\rangle/2}. \tag{10}$$

Finally, the exponent in the second exponential can be computed from the frequency noise power spectral density (PSD) as [29–32,43]

$$\langle\Delta\phi(\tau)^2\rangle/2 = 2\int_{-\infty}^{\infty} S_\nu(f)\frac{\sin(\pi f\tau)^2}{f^2}df, \tag{11}$$

where $S_\nu(f)$ is the **two-sided** frequency noise PSD in Hz^2/Hz. Note that most references plot the one-sided PSD (including here, in Fig. 3). The simplest result is for white noise, $S_\nu(f) = h_0$. This corresponds to an autocorrelation with pure exponential decay, whose Fourier transform is the Lorentzian function with FWHM $2\pi h_0$ (the "intrinsic" linewidth). Spontaneous emission is modeled as white noise, the magnitude of which is predicted by the well-known Schawlow-Townes equation. Strictly, because the spontaneous emission rate is dependent on gain at a given frequency, it is not truly white. However, most lasers exhibit gain bandwidths on the order of gigahertz to (many) terahertz, much wider than most single-frequency linewidths, and so the white noise approximation is appropriate. When the frequency noise PSD incorporates more complex features, the Fourier transform is generally not analytically solvable. With Eq. (8) it is straightforward to take an arbitrary measured frequency noise spectrum and numerically compute the effective lineshape. In the presence of $\propto 1/f^n$ "colored" noise, the spectrum takes on a Voigt structure, mixing Gaussian (near carrier) and Lorentzian (far from carrier). This results in a broader (near carrier), faster-decaying lineshape with more power concentrated at low offset frequencies. Other definitions such as the "integral" [37] or "beta-separation" [30] methods take the complex frequency noise into account in a prescribed manner. For white noise, all definitions converge to the same Lorentzian FWHM value.

Funding

U.S. Air Force (FA8721-05-C-0002); National Science Foundation (1122374).

Acknowledgments

G. N. West would like to thank Daniel Kramnik for helpful discussions on discrete time sampling and hardware implementations. This material is based upon work supported by the National Science Foundation Graduate Research Fellowship under Grant No. 1122374. The work at Lincoln Laboratory was sponsored by the Assistant Secretary of Defense for Research and Engineering under Air Force contract number FA8721-05-C-0002. Opinions, interpretations, conclusions, and recommendations are those of the authors and are not necessarily endorsed by the United States Government.

Disclosures

The authors declare no conflicts of interest.

References

1. W. Geng, C. Zhang, Y. Zheng, J. He, C. Zhou, and Y. Kong, "Stable quantum key distribution using a silicon photonic transceiver," Opt. Express **27**(20), 29045–29054 (2019).
2. J. Burke, "Atomic-photonic integration (a-phi) proposers' day," https://www.darpa.mil/attachments/PMA-PhI%2020180731_APhIProposersDay.pdf (2018).
3. K. K. Mehta, C. Zhang, M. Malinowski, T.-L. Nguyen, M. Stadler, and J. P. Home, "Integrated optical multi-ion quantum logic," Nature **586**(7830), 533–537 (2020).
4. R. Niffenegger, J. Stuart, C. Sorace-Agaskar, D. Kharas, S. Bramhavar, C. Bruzewicz, W. Loh, R. Maxson, R. McConnell, D. Reens, G. West, J. Sage, and J. Chiaverini, "Integrated multi-wavelength control of an ion qubit," Nature **586**(7830), 538–542 (2020).
5. N. H. Wan, T.-J. Lu, K. C. Chen, M. P. Walsh, M. E. Trusheim, L. De Santis, E. A. Bersin, I. B. Harris, S. L. Mouradian, I. R. Christen, E. S. Bielejec, and D. Englund, "Large-scale integration of artificial atoms in hybrid photonic circuits," Nature **583**(7815), 226–231 (2020).
6. C. Nguyen, D. Sukachev, M. Bhaskar, B. Machielse, D. Levonian, E. Knall, P. Stroganov, C. Chia, M. Burek, R. Riedinger, H. Park, M. Loncar, and M. Lukin, "An integrated nanophotonic quantum register based on silicon-vacancy spins in diamond," Phys. Rev. B **100**(16), 165428 (2019).
7. P. Kok, W. J. Munro, K. Nemoto, T. C. Ralph, J. P. Dowling, and G. J. Milburn, "Linear optical quantum computing with photonic qubits," Rev. Mod. Phys. **79**(1), 135–174 (2007).
8. G. N. West, W. Loh, D. Kharas, C. Sorace-Agaskar, K. K. Mehta, J. Sage, J. Chiaverini, and R. J. Ram, "Low-loss integrated photonics for the blue and ultraviolet regime," APL Photonics **4**(2), 026101 (2019).

9. T. Aellen, M. Giovannini, J. Faist, and J. P. Von Der Weid, "Feasibility study of free-space quantum key distribution in the mid-infrared," Quantum Inf. Comput. **8**, 0001–0011 (2008).
10. M. G. Thompson, A. Politi, J. C. Matthews, and J. L. O'Brien, "Integrated waveguide circuits for optical quantum computing," IET Circuits Devices Syst. **5**(2), 94–102 (2011).
11. J. Preskill, "Quantum computing in the nisq era and beyond," Quantum **2**, 7979 (2018).
12. E. Knill, "Quantum computing with realistically noisy devices," Nature **434**(7029), 39–44 (2005).
13. C. M. Gentry, "Scalable quantum light sources in silicon photonic circuits," Ph.D. thesis, University of Colorado at Boulder (2018). Section 5.2.
14. M. Piekarek, D. Bonneau, S. Miki, T. Yamashita, M. Fujiwara, M. Sasaki, H. Terai, M. G. Tanner, C. M. Natarajan, R. H. Hadfield, J. L. O'Brien, and M. G. Thompson, "High-extinction ratio integrated photonic filters for silicon quantum photonics," Opt. Lett. **42**(4), 815–818 (2017).
15. C. M. Gentry, O. S. Magaña-Loaiza, M. T. Wade, F. Pavanello, T. Gerrits, S. Lin, J. M. Shainline, S. D. Dyer, S. W. Nam, R. P. Mirin, and P. A. Milos, "Monolithic source of entangled photons with integrated pump rejection," in *2018 Conference on Lasers and Electro-Optics (CLEO)*, (IEEE, 2018), pp. 1–2.
16. N. C. Harris, D. Grassani, A. Simbula, M. Pant, M. Galli, T. Baehr-Jones, M. Hochberg, D. Englund, D. Bajoni, and C. Galland, "Integrated source of spectrally filtered correlated photons for large-scale quantum photonic systems," Phys. Rev. X **4**(4), 041047 (2014).
17. H.-K. Lo, X. Ma, and K. Chen, "Decoy state quantum key distribution," Phys. Rev. Lett. **94**(23), 230504 (2005).
18. T. Kawanishi, T. Sakamoto, M. Tsuchiya, M. Izutsu, S. Mori, and K. Higuma, "70 db extinction-ratio $LiNbO_3$ optical intensity modulator for two-tone lightwave generation," in *Optical Fiber Communication Conference*, (Optical Society of America, 2006), p. OWC4.
19. S. Liu, H. Cai, C. DeRose, P. Davids, A. Pomerene, A. Starbuck, D. Trotter, R. Camacho, J. Urayama, and A. Lentine, "High speed ultra-broadband amplitude modulators with ultrahigh extinction >65 dB," Opt. Express **25**(10), 11254–11264 (2017).
20. C. M. Wilkes, X. Qiang, J. Wang, R. Santagati, S. Paesani, X. Zhou, D. A. Miller, G. D. Marshall, M. G. Thompson, and J. L. O'Brien, "60 db high-extinction auto-configured mach–zehnder interferometer," Opt. Lett. **41**(22), 5318–5321 (2016).
21. S. I. El-Henawy, R. Miller, and D. S. Boning, "Effects of a random process variation on the transfer characteristics of a fundamental photonic integrated circuit component," in *Society of Photo-Optical Instrumentation Engineers (SPIE) Conference Series*, vol. 10743 (2018).
22. X. Wang, "Silicon photonic waveguide bragg gratings," Ph.D. thesis, University of British Columbia (2013).
23. J. Capmany, J. Marti, and H. Mangraham, "Impact of finite laser linewidth on the performance of ofdm networks employing single-cavity fabry-perot demultiplexers," J. Lightwave Technol. **13**(2), 290–296 (1995).
24. J. Martin and J. Capmany, "Transfer functions of double-and multiple-cavity fabry–perot filters driven by lorentzian sources," Appl. Opt. **35**(36), 7108–7111 (1996).
25. M. Rakhmanov, R. Savage Jr, D. Reitze, and D. Tanner, "Dynamic resonance of light in fabry–perot cavities," Phys. Lett. A **305**(5), 239–244 (2002).
26. O. Llopis, P.-H. Merrer, H. Brahimi, K. Saleh, and P. Lacroix, "Phase noise measurement of a narrow linewidth CW laser using delay line approaches," Opt. Lett. **36**(14), 2713–2715 (2011).
27. T. Okoshi, K. Kikuchi, and A. Nakayama, "Novel method for high resolution measurement of laser output spectrum," Electron. Lett. **16**(16), 630–631 (1980).
28. H. Welling and B. Wellegehausen, "High resolution michelson interferometer for spectral investigations of lasers," Appl. Opt. **11**(9), 1986–1990 (1972).
29. L. A. Coldren, S. W. Corzine, and M. L. Mashanovitch, *Diode lasers and photonic integrated circuits*, vol. 218 (John Wiley & Sons, 2012).
30. G. Di Domenico, S. Schilt, and P. Thomann, "Simple approach to the relation between laser frequency noise and laser line shape," Appl. Opt. **49**(25), 4801–4807 (2010).
31. G. N. West, "Visible and ultraviolet integrated photonics for addressing atomic systems," Master's thesis, Massachusetts Institute of Technology (2019). Chapters 1, 3.
32. K. Petermann, *Laser diode modulation and noise* (Kluwer Academic Publishers, 1988), chap. Noise characteristics of solitary laser diodes.
33. A. L. Schawlow and C. H. Townes, "Infrared and optical masers," Phys. Rev. **112**(6), 1940–1949 (1958).
34. Y. Fan, R. M. Oldenbeuving, C. G. Roeloffzen, M. Hoekman, D. Geskus, R. G. Heideman, and K.-J. Boller, "290 hz intrinsic linewidth from an integrated optical chip-based widely tunable inp-si3n4 hybrid laser," in *CLEO: QELS_Fundamental Science*, (Optical Society of America, 2017), pp. JTh5C–9.
35. C. T. Santis, S. T. Steger, Y. Vilenchik, A. Vasilyev, and A. Yariv, "High-coherence semiconductor lasers based on integral high-q resonators in hybrid si/iii-v platforms," Proc. Natl. Acad. Sci. **111**(8), 2879–2884 (2014).
36. D. Huang, M. A. Tran, J. Guo, J. Peters, T. Komljenovic, A. Malik, P. A. Morton, and J. E. Bowers, "High-power sub-khz linewidth lasers fully integrated on silicon," Optica **6**(6), 745–752 (2019).
37. D. R. Hjelme, A. R. Mickelson, and R. G. Beausoleil, "Semiconductor laser stabilization by external optical feedback," IEEE J. Quantum Electron. **27**(3), 352–372 (1991).
38. H. A. Haus, *Waves and fields in optoelectronics* (Prentice-Hall, 1984).

Optics EXPRESS

39. B. Ouyang, Y. Li, M. Kruidhof, R. Horsten, K. W. van Dongen, and J. Caro, "On-chip silicon mach–zehnder interferometer sensor for ultrasound detection," Opt. Lett. **44**(8), 1928–1931 (2019).
40. R. W. Fox, C. W. Oates, and L. W. Hollberg, "Stabilizing diode lasers to high-finesse cavities," in *Experimental methods in the physical sciences*, vol. 40 (Elsevier, 2003), pp. 1–46.
41. C. Panuski, D. Englund, and R. Hamerly, "Fundamental thermal noise limits for optical microcavities," arXiv preprint arXiv:2005.03533 (2020).
42. G. Huang, E. Lucas, J. Liu, A. S. Raja, G. Lihachev, M. L. Gorodetsky, N. J. Engelsen, and T. J. Kippenberg, "Thermorefractive noise in silicon-nitride microresonators," Phys. Rev. A **99**(6), 061801 (2019).
43. W. Loh, S. Yegnanarayanan, R. J. Ram, and P. W. Juodawlkis, "Unified theory of oscillator phase noise II: Flicker noise," IEEE Trans. Microwave Theory Tech. **61**(12), 4130–4144 (2013).
44. L. B. Mercer, "1/f frequency noise effects on self-heterodyne linewidth measurements," J. Lightwave Technol. **9**(4), 485–493 (1991).